Journal of Alloys and Compounds Communications 1 (2024) 100002

Contents lists available at ScienceDirect

Journal of Alloys and Compounds Communications

journal homepage: www.sciencedirect.com/journal/jacomc

Partial dislocation slip induced plasticity

Xiangyu Gao[a,1], Yan Wang[a,1], Jie Wang[a], Ying Ding[a], Xiaolin Li[b,*]

[a] Analytical & Testing Center, Northwestern Polytechnical University, Xi'an, Shaanxi 710072, PR China
[b] State Key Laboratory of Solidification Processing, Center of Advanced Lubrication and Seal Materials, Northwestern Polytechnical University, Xi'an, Shaanxi 710072, PR China

ARTICLE INFO

Keywords:
Twinning-induced plasticity
Transformation-induced plasticity
Partial dislocation slip
Full dislocation slip
Slip-induced plasticity

ABSTRACT

Both twinning and transformation can produce a macroscopic strain and cause a significant plastic deformation, which are known as twinning-induced plasticity (TWIP) and transformation-induced plasticity (TRIP), enhancing the plastic deformability of structural materials dramatically. As far as the authors believe, the underlying origin behind these kinds of plastic deformation should not be the twinning and transformation themselves. By deciphering microstructural origins of the two effects in a kind of interstitial high entropy alloy (iHEA), the slip of partial dislocations causing TWIP and TRIP is analogous to the full dislocation slip governing ductility of materials, determines the plastic deformation.

1. Introduction

The deformation mechanisms of metals have been studied for about 100 years, yielding a well-developed plasticity theory based on three principal mechanisms of dislocations [1,2], twins [3], grain boundary [4] and phase transitions [5]. Metals and alloys exhibit three corresponding deformation pathways, that is, dislocation -mediated plasticity, TWIP and TRIP involving a faced-centered-cubic (FCC) to hexagonal-closed-packed (HCP) transformation. The motion of dislocations can create plastic deformation. Dislocation motion mode can be changed from planar slip to cross slip via tunning chemical composition of structural materials [6–8], resulting in the further glide of dislocation and then increasing the tensile elongation. Tailoring the glide channel of dislocations by introducing the nano-twinning boundary (i.e., the easy motion of dislocation) can also generate significant ductility, enhancing the strength and plasticity of materials simultaneously [2,9–11].

In addition to the dislocation plasticity, the TWIP and TRIP effect can also overcome the strength-ductility trade-off. The stimulating of twinning in CrMnFeCoNi high-entropy alloy (HEA) is critical to enhancing the tensile ductility together with the higher strength at lower temperatures, which preserves the exceptional mechanical properties of this alloy at 77 K [3]. Deformation-stimulated martensitic transformation of FCC to HCP in dual phase HEA promotes the tensile elongation and leads to superior improvements in strength-ductility combinations compared to those obtained in conventional low-entropy systems [5]. All of the dislocation slip, TWIP and TRIP can create plastic deformation. So, is there any essential connection between the three deformation mechanisms? In this letter, the underlying origin of TWIP and TRIP will be disclosed through the deep analysis of the two effects occurring in a kind of iHEA, and the aforementioned question will be replied.

2. Experiment procedure

The nominal composition of the alloy is $Fe_{49.5}Mn_{29.7}Co_{9.9}Cr_{9.9}C_1$ (at %). The alloy ingot was prepared by vacuum melting and was homogenized at 1200 ℃ for 2 h in Ar atmosphere. The ingot was then hot-rolled into 3 mm plate and was cold-rolled into 1 mm plate. Dog bone-shaped tensile with a gauge length of 25 mm, a width of 6 mm and a thickness of 1.5 mm were prepared from the plate annealed at the temperatures of 800 ℃ for 1 h and followed by water quenching. Details of the material and experimental procedures can be found in [12]. A CMT5105 testing machine equipped with laser extensometer was employed for tensile tests at room temperature with a nominal strain rate of 10^{-3} s^{-1}, and the corresponding engineering stress-strain and strain hardening rate curves of the test iHEA are shown in Fig. 1. The yield strength, tensile strength and uniform elongation of the alloy are measured to be 526 MPa, 948 MPa and 35%, respectively. The test sample shows the steady strain hardening, as shown in Fig. 1(b). The deformation substructures of speicmens subjected to three interrupted tests at the strain of 2%, 20% and 35% were characterized by transmission electron microscopy (TEM), respectively.

* Corresponding author.
E-mail address: xiaolinli@nwpu.edu.cn (X. Li).
[1] Co-first author.

https://doi.org/10.1016/j.jacomc.2024.04.001
Received 8 February 2024; Received in revised form 17 March 2024; Accepted 1 April 2024
Available online 2 April 2024

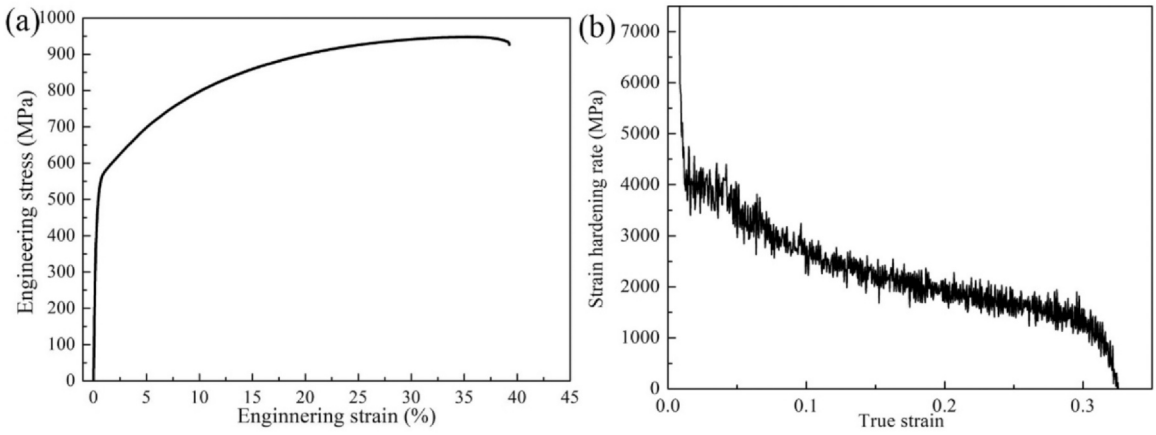

Fig. 1. (a) Engineering stress-strain curve of the test iHEA; (b) Strain hardening rate curve.

For TEM, disks of 3 mm diameter were punched out from thin foils of 50 μm thickness. Electron transparent samples for TEM investigation were electronpolished in dual-jet electropolisher using a solution of 9 vol% perchloric acid in ethanol at −15 ℃. TEM experiments were performed using an FEI Talos F200X microscope operating at 200 kV. Standard TEM techniques such as Bright-field (BF), selected area electron diffraction (SAED) and high resolution transmission electron microscopy (HRTEM) were used to characterize the microstructure.

3. Results and discussion

3.1. Microstructures

Fig. 2(a) shows a BF image of the tensile specimen interrupted at a strain of 2%, demonstrating some full dislocations marked by yellow arrows and some Shockly partials marked by red arrows gliding on the (111) plane, dragging a wide stacking-false (SF) behind them. The corresponding SAED pattern along $[10\bar{1}]$ zone axis of matrix in Fig. 2(d) reveals diffraction spots corresponding only to FCC structure. Upon increasing the strain level to 20%, lots of the thin lamellas shown in Fig. 2(b) were confirmed to be HCP phase by the HCP reflections in the associated SAED pattern viewed along $[10\bar{1}]_{FCC}//[11\bar{2}0]_{HCP}$ directions, as shown in Fig. 2(e). With increasing deformation to 35% strain, deformation twins appear in addition to HCP phase. Because of morphology similarity of the twins with HCP laths, it is difficulty to differentiate them, as shown in Fig. 2(c). However, the evidence for twins were clearly found in the associated SAED pattern recorded along $[10\bar{1}]_{FCC}//[11\bar{2}0]_{HCP}$ directions, as shown in Fig. 2(f).

To further investigate the transformation and twinning mechanisms, HRTEM examination was performed on samples deformed to 2%, 20%

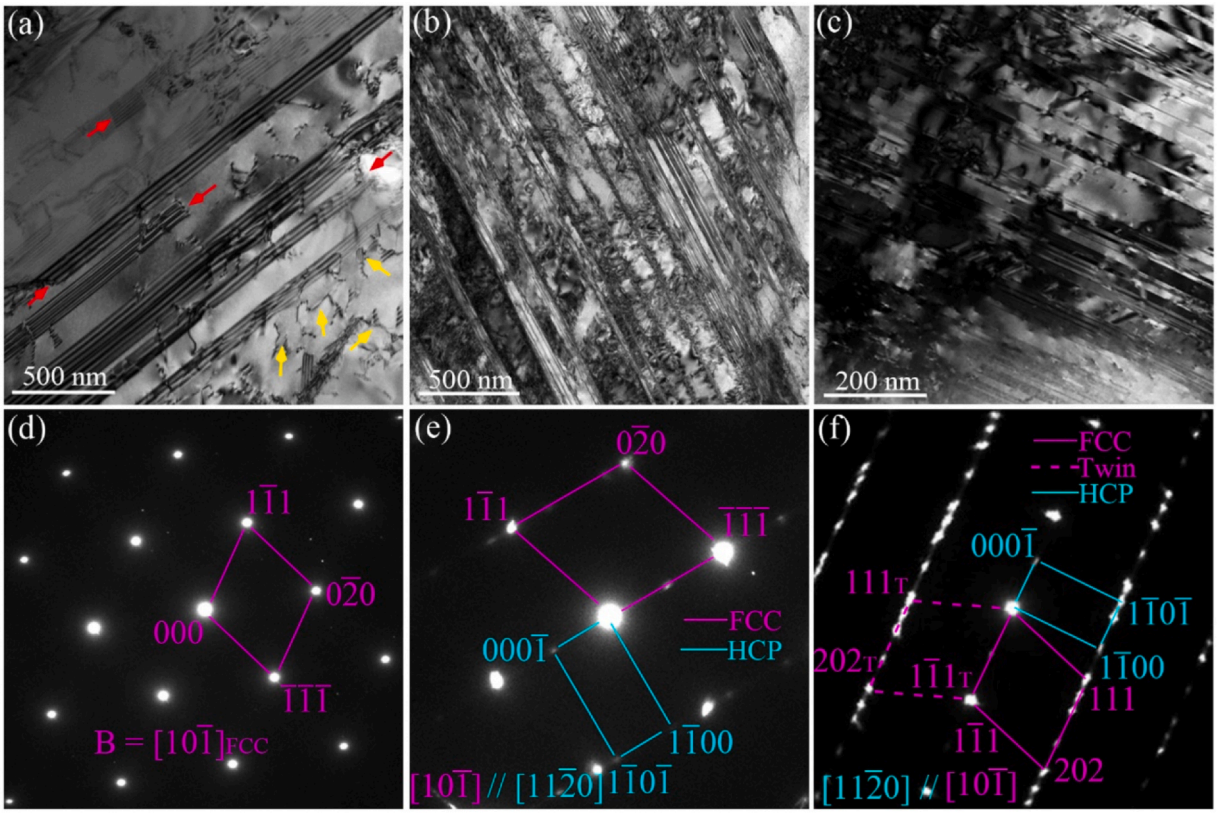

Fig. 2. BF images taken from the sample deformed to strain of (a) 2%, (b) 20% and (c) 35%, and the corresponding SAED patterns of (d), (e) and (f), respectively. Subscript T represents twin.

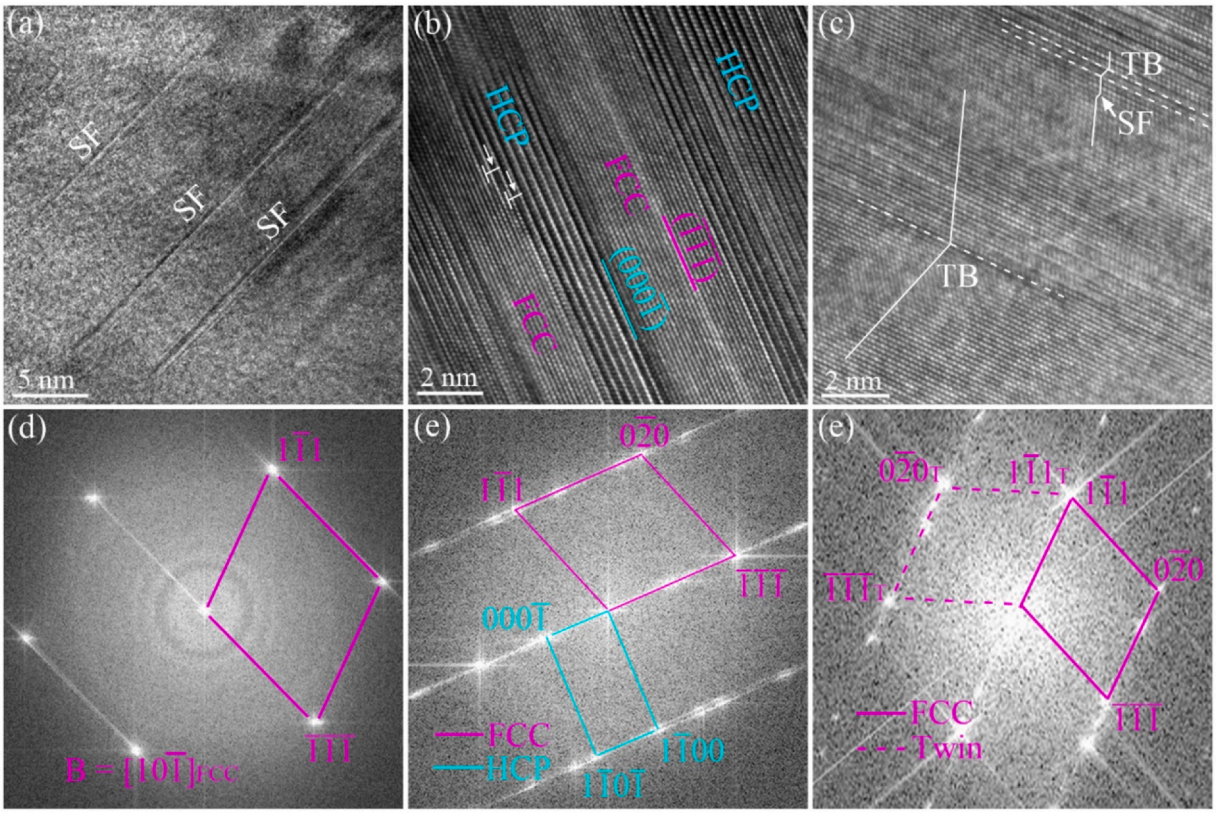

Fig. 3. HRTEM images taken from the sample deformed to strain of (a) 2%, (b) 20% and (c) 35%, and the corresponding FFT diffractograms of (d), (e) and (f), respectively. Subscript T represents twin.

and 35%, respectively. Fig. 3(a) shows a HRTEM image of the sample after strain of 2% and only SFs were found. The corresponding fast Fourier transformation (FFT) diffractogram revealed no extra secondary reflections except for those corresponding to FCC structure, as shown in Fig. 3(d). For the sample at a strain of 20%, the lattice image and the corresponding FFT diffractogram are shown in Fig. 3(b) and Fig. 3(e), respectively. According to the FFT diffractogram, FCC and HCP laths have an orientation relationship of $[10\bar{1}]_{FCC}//[11\bar{2}0]_{HCP}$ and $(\bar{1}\bar{1}\bar{1})_{FCC}//(000\bar{1})_{HCP}$. Shockley partial dislocations marked by white arrows glided at the edge of HCP laths, creating new stacking faults and leaving HCP laths behind, as shown in Fig. 3(b). The HRTEM image shown in Fig. 3(c) and the corresponding FFT diffractogram along $[10\bar{1}]$ direction shown in Fig. 3(f) reveal extensive deformation twinning in the sample deformed to 35% strain.

According to the results in Fig. 2 and Fig. 3, at low strain of 2%, deformation was mainly carried by dislocation motion and SFs. SFs are likely to act as nuclei of twinning and HCP phase [13,14]. With the increase of strain to 20%, TRIP effect of FCC to HCP was activated. Increasing the deformation strain to 35% triggers the TWIP effect while mainting the TRIP effect. Dislocation slip, SFs, TRIP and TWIP effects are all able to carry the plastic deformation of the alloy. Is there any similar undlying cause of these deformation modes? This question will be replied by deeply analyzing the mechanisms of these modes

3.2. Deformation mechanism

The excellent mechanical properties of TWIP metals and alloys can be attributed to the formation of deformation twins during plastic deformation [15–17]. Therefore, twin formation mechanisms have been a focus of research. Twining mechanism via partial dislocation emission from free surfaces, grain boundaries and grain boundary junctions on consecutive {111} planes shown in Fig. 4(a-d), has been experimentally verified in both nc and coarse-grained metals[18–22]. Fig. 4(a) shows the arrangement of atoms on $(10\bar{1})_{fcc}$ plane before twinning. Fig. 4(b) shows a Shockley partial dislocation with a Burgers vector of $\frac{1}{6}[1\bar{2}1]$ emitted from the grain boundary and gliding within the grain with the displacement of $\frac{1}{6}[1\bar{2}1]$, trailing a SF behind it, similar to that in Fig. 3(c). Fig. 4(c) and (d) show the second and third partial dislocations are emitted on consecutive (111) planes and glide on it with the displacement of $\frac{2}{6}[1\bar{2}1]$ and $\frac{3}{6}[1\bar{2}1]$ respectively, making the twin grow two and three atomic layer planes. In this mechanism, Shockley partial is gliding on a (111) plane, one at a time and one after another. With further deformation, successive partial dislocations with the same Burgers vector are emitted and glide on consecutive twinning (111) planes, a twin forms and the grain experienced a global shear strain displacement of $\frac{n}{6}[1\bar{2}1]$.

Since deformation twinning produce a macroscopic strain and cause a significant plastic deformation, we call this effect as the twinning induced plasticity. However, from the schematic twinning mechanisms shown in Fig. 4, deformation twinning is attributed to the slip of the partial dislocation. Therefore, twinning induced plasticity is essentially the partial dislocation slip induced plasticity.

For FCC metals and alloys, there is another quite important deformation mechanism referred to as TRIP effect [23–26], occurring in this alloy deformed to 20%. This mechanism is enabled by triggering transformation from a FCC matrix into a HCP structure. Is the slip induced plasticity that we propose suitable for TRIP effect? Analyzing and comparing the FCC and the HCP structure is beneficial to reveal the deformation mechanism and then to answer this question. Although the FCC and the HCP structures are quite different from each other based on their crystal cells shown in Fig. 5(a) and Fig. 5(d), an identical characteristics still exists, i.e., both structures can be deemed as a stacking of the same closed packed plane, (111) plane for FCC structure and (0001) plane for HCP, as shown in Fig. 5(b) and Fig. 5(d). The FCC structure has a crystal characteristic of ABCABC stacking sequence shown in Fig. 5(a-c), while the HCP structure has one of ABAB sequence shown in Fig. 5(d-e). A layer atom has a displacement of $\frac{1}{6}$ < 121> with

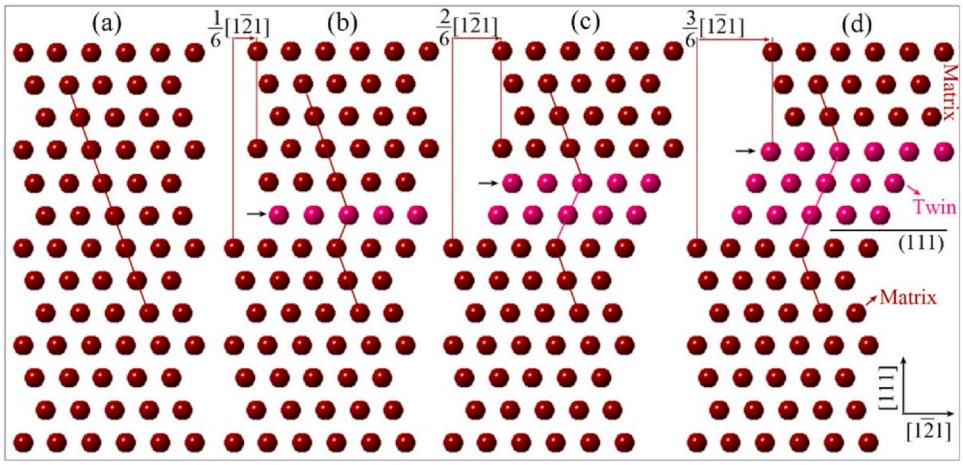

Fig. 4. (a) Arrangement of atoms of FCC structure on $(10\bar{1})_{fcc}$ plane without any defects. (b), (c) and (d) Showing the first, second and third partial dislocations with Burgers vector of $\frac{1}{6}[1\bar{2}1]$ are emitted on consecutive (111) planes and glide on it with the displacement of $\frac{1}{6}[1\bar{2}1]$, $\frac{2}{6}[1\bar{2}1]$ and $\frac{3}{6}[1\bar{2}1]$, respectively.

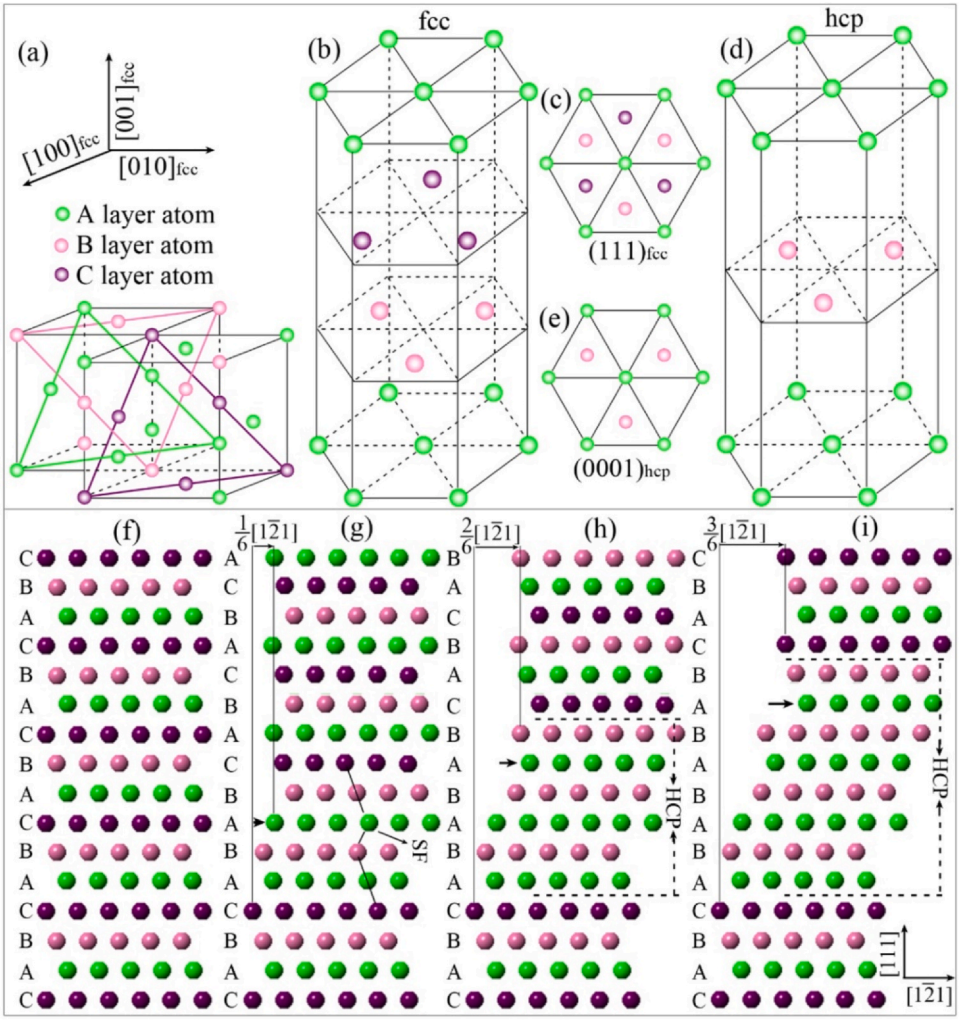

Fig. 5. (a) Two FCC crystal cells next to each other representing stacking sequence of (111) plane. (b) FCC crystal cell represented with HCP crystal axis. (c) Atomic projection of FCC structure on (111) close-packed plane. (d) HCP crystal cell. (e) Atomic projection of HCP structure on (0001) close-packed plane. (f-i) Schematic illustration of FCC-HCP phase transformation mechanism. (f) Stacking sequence of FCC structure on $(10\bar{1})_{fcc}$ plane without any stacking false. (g) A stacking false is formed by the slip of the Shockley partial with the Burgers vector of $\frac{1}{6}[1\bar{2}1]$ on (111) plane. (h) and (i) Showing the second and third partial dislocations with the same Burgers vector gliding on every second (111) planes, results in a six and eight layers atomic ABAB stacking sequence, respectively.

respect to B layer atom, which is suitable for B layer atom relative to C layer atom. Therefore, the transformation of FCC to HCP is changed to the conversion of ABCABC sequence to ABAB sequence.

Fig. 5(f-i) shows the schematic of the transformation mechanism. A slab with the FCC structure was created by sequentially stacking 16 closed-packed (111) atomic planes, as shown in Fig. 5(f). Then, an

intrinsic stacking fault was created by shifting the top 10 layers along the $[1\bar{2}1]$ direction via the glide of the first Shockley partial with the Burgers vector of $\frac{1}{6}[1\bar{2}1]$ on (111) plane. This results in a SF and two ABAB stacking sequence with HCP coordination, as shown in Fig. 5(g). Subsequent displacement of the top eight and six layers in Fig. 5(h) and Fig. 5(i) along the $[1\bar{2}1]$ direction results in a three and four ABAB stacking sequence, respectively. This can proceed with second and third partial dislocations gliding on every second (111) plane with the displacement of $\frac{2}{6}[1\bar{2}1]$ and $\frac{3}{6}[1\bar{2}1]$, as shown in Fig. 5(h) and Fig. 5(i), respectively. As such, continued shifting of the crystal via Shockley partials slipping on every other (111) plane will create a HCP structure shown in Fig. 3(b), and the crystal experienced a global shear strain displacement of $\frac{n}{6}[1\bar{2}1]$, which is similar to the deformation twinning. Transformation of FCC to HCP caused a dramatic plastic deformation and then this effect was referred to as transformation induced plasticity. Nonetheless, transformation is also because of the slip of the partial dislocation judging from the schematic transformation mechanism shown in Fig. 5. It is, therefore, can be concluded that not the twinning or/and transformation but the partial dislocation slip produce the plastic strain and then the ductility.

From all the mentioned above, both TWIP and TRIP are all partial dislocation slip induced plasticity. So strictly speaking, it is not the twinning or/and transformation but the slip of partial dislocations determined the deformation of materials and then the plasticity. Therefore, the essence behind the plasticity is slip of either full or partial dislocation. The slip induced plasticity obtained from the analysis of TWIP and TRIP is also suitable for microband-induced plasticity (MBIP) [27–30] and stacking-faults-induced plasticity (SFIP) [31,32]. It is only due to the discovery of the microbands and stacking-faults during the deformation of metals and alloys, MBIP and SFIP were proposed. However, the occurrence of microbands was ascribed to the multi-slip process of full dislocation [28], while the appearance of stacking-faults was attributed to the slip of Shockley partial dislocation with a Burgers vector of $\frac{1}{6}[1\bar{2}1]$ on the closed packed plane shown in Fig. 4(c) and Fig. 5(g). Therefore, all of the XX-induced plasticity are essentially slip-induced plasticity (SLIP).

4. Conclusion

The underlying origin behind TWIP and TRIP effects occurring in a kind of iHEA has been deeply analysed, the main findings in the present study are summarized as follows.

1. It is the slip of line defects involving full and partial dislocations determined the plasticity of metals and alloys, according to the deep analysis of TWIP and TRIP effects occurring in this iHEA together with the dislocation plasticity.
2. The slip of line defects can make the structural materials experience a global shear strain displacement of Burgers vector of full or partial dislocations, and then produce a macroscopic strain and cause a significant plastic deformation.
3. The slip of line defects is the cause of the all XX-induced plasticity which also can be called SLIP.

CRediT authorship contribution statement

Xiangyu Gao: Conceptualization, Methodology, Investigation, Writing – original draft. **Yan Wang:** Conceptualization, Writing. **Jie Wang:** Methodology. **Ying Ding:** Methodology. **Xiaolin Li:** Conceptualization, Supervision, Writing – original draft.

Data availability

Data will be made available on request.

Declaration of Competing Interest

The authors declare that they have no known competing financial interests or personal relationships that could have appeared to influence the work reported in this paper.

Acknowledgements

The authors are grateful for the Natural Science Foundation of China (No. 52374403 and 52004224) and Scientific and Technological Program of Shaanxi Province (No. 2019PT-06).

References

[1] M.J. Lai, C.C. Tasan, D. Raabe, Acta Mater. 100 (2015) 290–300.
[2] Z.J. Zhang, H.W. Sheng, Z.J. Wang, B. Gludovatz, Z. Zhang, E.P. George, Q. Yu, S.X. Mao, R.O. Ritchie, Nat. Commun. 8 (2017) 14390.
[3] B. Gludovatz, A. Hohenwarter, D. Catoor, E.H. Chang, E.P. George, R.O. Ritchie, Science 345 (2014) 1153–1158.
[4] L. Lu, M.L. Sui, K. Lu, Science 287 (2000) 1463–1466.
[5] Z.M. Li, K.G. Pradeep, Y. Deng, D. Raabe, C.C. Tasan, Nature 534 (2016) 227–230.
[6] Z.F. Lei, X.J. Liu, Y. Wu, H. Wang, S.H. Jiang, S.D. Wang, X.D. Hui, Y.D. Wu, B. Gault, P. Kontis, D. Raabe, L. Gu, Q.H. Zhang, H.W. Chen, H.T. Wang, J.B. Liu, K. An, Q.S. Zeng, T.G. Nieh, Z.P. Lu, Nature 563 (2018) 546–550.
[7] Q.Q. Ding, Y. Zhang, X. Chen, X.Q. Fu, D.K. Chen, S.J. Chen, L. Gu, F. Wei, H.B. Bei, Y.F. Gao, M.R. Wen, J.X. Li, Z. Zhang, T. Zhu, R.O. Ritchie, Q. Yu, Nature 574 (2019) 223–227.
[8] Y. Chong, R.P. Zhang, M.S. Hooshmand, S.T. Zhao, D.C. Chrzan, M. Asta, J.W. Morris Jr, A.M. Minor, Nat. Commun. 12 (2021) 6158.
[9] L. Lu, Y.F. Shen, X.H. Chen, L.H. Qian, K. Lu, Science 16 (2004) 422–426.
[10] K. Lu, L. Lu, S. Suresh, Science 324 (2009) 349–352.
[11] L. Lu, X. Chen, X. Huang, K. Lu, Science 323 (2009) 607–610.
[12] X.L. Li, X.X. Hao, C. Jin, Q. Wang, X.T. Deng, H.F. Wang, Z.D. Wang, J. Mater. Sci. Technol. 110 (2022) 167–177.
[13] Y. Deng, C.C. Tasan, K.G. Pradeep, H. Springer, A. Kostka, D. Raabe, Acta Mater. 94 (2015) 124–133.
[14] Z.M. Li, C.C. Tasan, H. Springer, B. Gault, D. Raabe, Sci. Rept. 7 (2017) 40704.
[15] M.X. Yang, D.S. Yana, F.P. Yuan, P. Jiang, E. Mac, Xl Wu, PNAS 115 (2018) 7224–7229.
[16] P.J. Shi, Y.B. Zhong, Y. Li, Wl Ren, T.X. Zheng, Z. Shen, B. Yang, J.C. Peng, P.F. Hu, Y. Zhang, P.K. Liaw, Y.T. Zhu, Mater. Today 41 (2020) 62–71.
[17] S.T. Zhao, R.P. Zhang, Q. Yu, J. Ell, R.O. Ritchie, A.M. Minor, Science 373 (2021) 1363–1368.
[18] J.K. Kim, M.H. Kwon, B.C. De Cooman, Acta Mater. 141 (2017) 444–455.
[19] C.X. Huang, K. Wang, D. Wu, Z.F. Zhang, G.Y. Li, S.X. Li, Acta Mater. 54 (2006) 655–665.
[20] Y.F. Shen, Y.D. Wang, X.P. Liu, X. Sun, R.L. Peng, S.Y. Zhang, L. Zuo, P.K. Liaw, Acta Mater. 61 (2013) 6093–6106.
[21] J.W. Christian, S. Mahajan, Prog. Mater. Sci. 39 (1995) 1–157.
[22] A.J. Cao, Y.G. Wei, S.X. Mao, Appl. Phys. Lett. 90 (2007) 15909.
[23] J. Wang, H. Huang, Appl. Phys. Lett. 85 (2004) 5983.
[24] W.J. Lu, C.H. Liebscher, G. Dehm, D. Raabe, Z.M. Li, Adv. Mater. (2018) 1804727.
[25] Xl An, Z.W. Wang, S. Ni, M. Song, Sci. China Mater. 63 (2018) 1797–1807.
[26] U.F. Kocks, A.S. Argon, M.F. Ashby, Prog. Mater. Sci. 19 (1975) 1–281.
[27] Z.W. Wang, I. Baker, W. Guo, J.D. Poplawsky, Acta Mater. 126 (2017) 346–360.
[28] Z.W. Wang, I. Baker, Z.H. Cai, S. Chen, J.D. Poplawsky, W. Guo, Acta Mater. 120 (2016) 228–239.
[29] M. Song, R. Zhou, J. Gu, Z.W. Wang, S. Ni, Y. Liu, Appl. Mater. Today 18 (2020) 100498.
[30] T. Yang, Y.L. Zhao, Y. Tong, Z.B. Jiao, J. Wei, J.X. Cai, X.D. Han, D. Chen, A. Hu, J.J. Kai, K. Lu, Y. Liu, C.T. Liu, Science 362 (2018) 933–937.
[31] Q.S. Pan, L.X. Zhang, R. Feng, Q.H. Lu, K. An, A.C. Chuang, J.D. Poplawsky, P.K. Liaw, L. Lu, Science 374 (2021) 984–989.
[32] Q.S. Pan, M.X. Yang, R. Feng, A.C. Chuang, K. An, P.K. Liaw, X.L. Wu, N.R. Tao, L. Lu, Science 382 (2023) 185–190.